

₁ Electrical Signature of the ₂ Percolation Threshold in Sea Ice

Kenneth M. Golden¹, Hajo Eicken², Adam Gully¹, Malcolm Ingham³,
Keleigh A. Jones⁴, Joyce Lin⁵, James E. Reid⁶,
Christian S. Sampson¹, and Anthony P. Worby⁷

Corresponding author: Kenneth M. Golden, University of Utah, Department of Mathematics,
155 S 1400 E, RM 233, Salt Lake City, UT 84112-0090, USA. (golden@math.utah.edu)

¹University of Utah, Department of

3 ABSTRACT: Fluid flow through sea ice governs a broad range of geophys-
 4 ical and biological processes in the polar marine environment. For example,
 5 the evolution of melt ponds and sea ice albedo, which is important in climate
 6 modeling, is constrained by drainage through the porous brine microstruc-

Mathematics, 155 S 1400 E, RM 233, Salt

Lake City, UT 84112-0090, USA.

(golden@math.utah.edu)

²University of Alaska Fairbanks,
 Fairbanks, AK 99775-7320, USA.

³School of Chemical and Physical
 Sciences, Victoria University of Wellington,
 P.O. Box 600, Wellington, NZ.

⁴GNS Science, 1 Fairway Drive, Avalon
 5010, PO Box 30-368, Lower Hutt 5040, NZ.

⁵California Polytechnic State University,
 Department of Mathematics, San Luis
 Obispo, CA 93407-0403

⁶Mira Geoscience, 45 Ventnor Ave., West
 Perth, WA 6005, AU.

⁷Antarctic Climate & Ecosystems CRC,
 Private Bag 80, Hobart, Tasmania 7001 AU.

7 ture. However, for brine volume fractions below about 5%, columnar sea ice
8 is effectively impermeable to fluid flow. In two different experiments conducted
9 in the Arctic and Antarctic, we have found that this critical fluid transition
10 exhibits a strong electrical signature, with sea ice resistivity rising sharply
11 over three orders of magnitude near the brine connectivity threshold. The
12 data are accurately explained by percolation theory, with the same univer-
13 sal critical exponent which captures fluid permeability. These results enable
14 us to connect specific electrical profiles to important processes such as melt
15 pond formation and drainage, CO₂ pumping, and the flux of nutrients which
16 sustain biomass build-up.

Key Points:

1. Data on the electrical resistivity of sea ice were taken in the Arctic and Antarctic.
2. A strong electrical response near the brine percolation threshold is observed and explained theoretically.
3. The results enable non-destructive and remote monitoring of key sea ice processes and transitions.

1. Introduction

Polar sea ice is a key component of Earth's climate system, and a leading indicator of climate change [Meier *et al.*, 2014; Thomas and Dieckmann, 2009; Serreze *et al.*, 2007]. As a material sea ice is a composite of pure ice with brine and air inclusions. The brine phase hosts extensive microbial communities which sustain life in the polar oceans [Thomas and Dieckmann, 2009; Fritsen *et al.*, 1994]. Fluid flow through the porous microstructure mediates key processes impacting the climatology and biology of sea ice. Improving projections of the fate of Earth's sea ice cover and its ecosystems depends on a better understanding of these important processes and feedback mechanisms.

For example, the evolution of sea ice albedo represents a fundamental problem in climate modeling and a significant source of uncertainty in climate projections [Flocco *et al.*, 2010; Polashenski *et al.*, 2012]. The albedo of sea ice floes is determined by melt pond evolution [Perovich *et al.*, 2002; Polashenski *et al.*, 2012]. Drainage of the ponds, with a resulting increase in albedo, is largely controlled by the fluid permeability of the porous sea ice underlying the ponds [Eicken *et al.*, 2004; Golden *et al.*, 2007]. As ice recedes with melting, more water surface is exposed, which increases solar absorption, leading in turn

to more melting, and so on. This *ice–albedo feedback* has played a significant role in the decline of the summer Arctic ice pack [Pistone *et al.*, 2014; Perovich *et al.*, 2007].

Fluid flow through sea ice governs the evolution of the salt budget and salinity profiles [Thomas and Dieckmann, 2009], convection-enhanced thermal transport [Lytle and Ackley, 1996], ocean-ice-atmosphere CO₂ exchanges [Loose *et al.*, 2011], and the build-up of algal biomass fueled by nutrient fluxes [Thomas and Dieckmann, 2009; Fritsen *et al.*, 1994]. It also drives snow-ice formation, accounting for a significant portion of the ice produced in the Southern Ocean [Maksym and Markus, 2008]. Sea water percolates upward through the porous microstructure, flooding the snow layer, and subsequently freezing.

While fluid flow is substantially restricted for brine volume fractions ϕ below about 5%, columnar sea ice is increasingly permeable for ϕ above 5% [Golden *et al.*, 1998]. For a typical bulk salinity of 5 ppt, the critical porosity $\phi_c \approx 5\%$ corresponds to a temperature $T_c \approx -5^\circ$ C. This critical behavior of the fluid permeability, which is known as the *rule of fives*, results from a connectivity or percolation threshold in the brine microstructure [Golden *et al.*, 1998, 2007; Pringle *et al.*, 2009].

If the fluid transport properties of sea ice can be linked to its electrical properties, which is the aim of this paper, then new approaches can be brought to bear in monitoring the state of sea ice. For example, it could open the door to the development of sensors to enhance existing buoy networks, provide information on key ice processes, and improve integration with satellite data.

The electrical conductivity of sea ice has been studied over the past five decades [Fujino and Suzuki, 1963; Addison, 1969; Thyssen *et al.*, 1974; Buckley *et al.*, 1986; Reid *et al.*,

2006; *Ingham et al.*, 2008]. However, there have been no observations of critical behavior in electrical properties corresponding to the microstructural transition encapsulated in the rule of fives. Here we report on two types of experiments where electrical resistivity data clearly display critical behavior at the brine percolation threshold. The mathematical description we develop provides a rigorous link between fluid and electrical transport in sea ice, with both displaying the same type of universal critical behavior, thus laying the foundation for the techniques referred to above. In fact, we further develop this foundation by partitioning the range of resistivity values of our data into intervals which correspond to distinct regimes of fluid permeability characteristics and related process behavior, such as melt pond development, and fluxes of nutrients and CO₂.

One of the goals of this work is to obtain data on the linkages between electrical and hydraulic properties [*Wong*, 1988]. The value of such an approach lies in the potential to then extract information about other key variables describing the state of sea ice, e.g., pertaining to its rheology or potential to harbor microbial communities. Our results indicate that such information could potentially be obtained from measurements of electric properties via *in situ* drifting sensors that can monitor the evolution of sea ice non-destructively (Figure 1 d).

The findings presented here also have implications for measuring ice thickness, an important gauge of the impact of climate change. Not only is thickness data important in comparing climate model predictions to observed behavior, but in specifying the initial conditions necessary for long-term numerical simulations. Promising techniques for advanced airborne or surface-based measurements of ice thickness depend on the interaction

of electromagnetic (EM) fields with sea ice. For example, there has been significant interest in the development of EM induction devices [Haas, 2004; Reid *et al.*, 2006] mounted on ships, planes and helicopters. These techniques, and the interpretation of the data to obtain thickness information, rely on knowledge of the electrical properties of sea ice, and how they vary with depth, temperature, salinity, and ice type. The results presented here shed significant light on such issues.

2. Measuring the electrical properties of sea ice

Sea ice is an anisotropic composite with vertically elongated brine inclusions and corresponding anisotropy in the effective fluid permeability and electrical conductivity tensors. Most methods for measuring sea ice conductivity involve indirect or inverse techniques, such as surface-based geoelectric profiling using a Wenner array of electrodes [Fujino and Suzuki, 1963; Thyssen *et al.*, 1974; Buckley *et al.*, 1986; Reid *et al.*, 2006; Ingham *et al.*, 2008; Sampson *et al.*, 2011]. Generally with these methods the vertical conductivity σ_v^* is inherently mixed with the horizontal components. Here we are most interested in σ_v^* due to its connection with vertical fluid flow.

During the Sea Ice Physics and Ecosystem Experiment (SIPEX) in September and October of 2007, we made *direct* measurements of σ_v^* in Antarctic pack ice by adapting a four probe Wenner array for use in cylindrical ice cores, as shown in Figure 1 a and b. The study area was located off the coast of East Antarctica, between 115° E and 130° E, and 64° S and 66° S. At 8 of the 15 ice stations along the cruise track of the Australian icebreaker *Aurora Australis*, we extracted vertical cores from thin first-year sea ice, with lengths ranging from 34 cm to 86 cm. Thermistor probes were inserted into small holes

drilled every 5 cm. We used a Wenner electrode array along sections of the cores, connected to a YEW Earth Resistance Tester operating at 38 Hz. This set-up yields the resistance along the axis of the cylindrical ice core between probes P1 and P2, corresponding to the vertical direction *in situ*, with $a = L = 10$ cm (or $a = L = 5$ cm in some cases). We obtained 26 averaged data points from 67 raw measurements of the resistance between the inner probes. After the temperature and resistance measurements were taken, which took about 10 to 20 minutes, we cut each core into 10 cm sections which were later melted, so that we could obtain bulk salinity measurements for each section. The temperature and salinity measurements allowed us to calculate a brine volume fraction profile for each core [Petrich and Eicken, 2009].

In the Arctic, we used the technique of cross-borehole DC resistivity tomography [Ingham *et al.*, 2008; Jones *et al.*, 2010], as shown in Figure 1 c and d. The ice is probed in its natural state, utilizing two or four vertical strings of electrodes frozen into the ice. It has been shown that this method can be used to derive the horizontal component of the anisotropic resistivity profile. Moreover, it has been demonstrated that the vertical component of σ^* can be obtained as well [Jones *et al.*, 2010; Ingham *et al.*, 2008]. If a minimum of four electrode strings are used, the geometric mean of the vertical and horizontal components of σ^* can be derived, along with the horizontal component [Ingham *et al.*, 2008], yielding the vertical component.

Measurements of the temporal variation in the resistivity structure of first-year Arctic sea ice through spring warming have been made approximately 1 km off the coast of Barrow, Alaska at $71^\circ 21' 56.45''$ N, $156^\circ 32' 39.01''$ W. Electrode strings were installed in

landfast first year ice in late January 2008. Cross-borehole measurements were made on 6
 separate occasions between early April and mid June 2008, allowing both the horizontal
 and vertical components of the ice resistivity to be derived. A sea ice mass balance
 site and an ice core sampling program at the same location [Druckenmiller *et al.*, 2009]
 provided ice temperature and salinity data, allowing the variation in resistivity structure
 to be correlated with brine volume fraction ϕ .

3. Modeling the electrical conductivity of sea ice

Lattice and continuum percolation models [Stauffer and Aharony, 1992] have been used
 to study a broad range of disordered materials where the connectedness of one phase
 dominates effective transport behavior. In sea ice, the fluid and electrical transport prop-
 erties are largely determined by the connectedness of the brine phase – an electrically
 conducting fluid.

Consider the two dimensional square network of bonds (edges) joining nearest neighbor
 sites (vertices) in the integer lattice, as shown in Figure 2 a and b. The bonds are
 assigned electrical conductivities $\sigma_0 > 0$ (open) or 0 (closed) with probabilities p and
 $1 - p$, so that a relative proportion p of the bonds are open. The *percolation threshold* p_c
 is the smallest value of p for which an infinite, connected cluster of open bonds forms. In
 two dimensions ($d = 2$), $p_c = \frac{1}{2}$, and in three ($d = 3$), $p_c \approx 0.25$. For p above but near
 the percolation threshold, the effective or bulk conductivity $\sigma^*(p)$ is believed to display
 power law behavior,

$$\sigma^*(p) \sim \sigma_0(p - p_c)^t, \quad (1)$$

where t is the conductivity critical exponent. For lattices, t is believed to be universal, depending only on dimension and not, for example, on whether the lattice is square or triangular. In $d = 2$, $t \approx 1.3$, and in $d = 3$, $t \approx 2.0$ [Stauffer and Aharony, 1992]. The effective resistivity is given by $\rho^*(p) = 1/\sigma^*(p)$.

In applying percolation theory to sea ice, it is useful to consider the vertical conductivity formation factor $F = \sigma_v^*/\sigma_b$, which removes the dependence of the effective parameter on the changing conductivity σ_b of the brine. In view of (1),

$$F(\phi) \sim F_0 (\phi - \phi_c)^2, \quad (2)$$

with $\phi_c \approx 0.05$ and $t \approx 2.0$, the $d = 3$ universal lattice value.

The scaling factor F_0 is obtained by relating the electrical conductivity to the fluid permeability of sea ice through a critical (or *bottleneck*) radius r_c [Friedman and Seaton, 1998]. By measuring the radii of vertical pathways in X-ray tomography images [Golden et al., 2007; Pringle et al., 2009], we estimate a range in mm of $0.1 \leq r_c \leq 0.2$, yielding a range for F_0 of $6 \leq F_0 \leq 24$. The relations between fluid and electrical transport in sea ice and the formula for F_0 are developed in the supplemental material.

4. Comparison of theory and data

In order to compare our conductivity measurements with percolation theory, we must exclude data below $\phi_c \approx 0.05$ [Golden et al., 2007], since the theory is only valid for $\phi > \phi_c$. It is more illustrative to display the data in terms of the reciprocal $G = 1/F = \rho_v^*/\rho_b$, which is the vertical resistivity formation factor. As the conductivity F becomes very small near ϕ_c , its reciprocal G becomes very large, with its behavior approximating a vertical asymptote near $\phi = \phi_c$. In Figure 2 c and d we show the two data sets from the

Antarctic and Arctic. By fixing the exponent $t = 2$ and the threshold value $\phi_c = 0.05$ in the above expression for $F(\phi)$, a statistical best fit of the data yields a value of $F_0 \approx 9$, which lies inside our predicted range, so that $F(\phi) \sim 9 (\phi - 0.05)^2$.

We see that the data agree well with the theory, and that they both exhibit divergent behavior with a vertical asymptote at the percolation threshold. Moreover, in the variables $x = \log(\phi - 0.05)$ and $y = \log F$, the line predicted by percolation theory is $y = 2x + \log F_0$, with $\log F_0 = 0.95$, $F_0 = 9$. Critical path analysis yields the bounds $0.8 \leq \log F_0 \leq 1.4$, and the best fit for the Antarctic data in f is $y = 1.99x + 0.93$, where 0.93 lies inside these bounds. In logarithmic variables, the error of the regression is 0.38 for the Arctic data and 0.22 for the Antarctic data (that is, approximately 68% of the Antarctic data is within 0.22 of the regression line). The increased scatter in the Arctic data is not surprising given the inverse computation required.

5. Discussion

Figure 3 illustrates how we can derive information about the permeability structure and relevant transport processes from resistivity soundings of Arctic sea ice with *in situ* electrode strings [Jones *et al.*, 2010]. Thus, the different formation factor regimes shown correspond to different permeability classes, with the lowermost ice layers permeable enough to allow for gas and nutrient exchange conducive to biomass build-up and CO₂ pumping [Loose *et al.*, 2011; Rysgaard *et al.*, 2007], based on a critical permeability of 4×10^{-11} m², corresponding to a resistivity formation factor of 31.3 for $r_c = 0.1$ mm. This permeable base layer increases in vertical extent as the ice warms and thins due to bottom and surface melt. The ice interior is permeable enough to allow for meltwater flushing

and reduction of ice salinity at surface ablation rates of 10 cm/d or less even prior to the onset of melt [Freitag and Eicken, 2003], corresponding to a resistivity formation factor of 625. High resistivity formation factors near the top in Figure 3 b are in part explained by such percolation of freshwater below accumulations of surface melt water.

Let us further examine how our results may be used to provide a better understanding of key processes like melt pond evolution. Incorporating such processes into climate models is critical to improving projections of climate change. Development and tuning of improved climate models could be significantly enhanced by ground truth information and monitoring of these key processes and the internal state of the sea ice.

For example, there is recent evidence from Arctic sea ice experiments (conducted by C. Polashenski and K. M. Golden in 2014) that percolation of freshwater from snowmelt into the upper layers of sea ice, and its subsequent freezing, could be fundamental to the very formation of melt ponds. This process reduces the permeability – thus increasing the electrical resistivity, a process likely to have a recognizable electrical signature, as evidenced in Figure 3. Gauging the impact, for example, of changing Arctic snowfall on the availability of freshwater for melt pond formation could be made possible with methods based on our results. Melt pond drainage events, which can have a significant impact on sea ice albedo, often follow an increase in permeability through its percolation threshold, which has a strong electrical signature. Specific information on electrical and fluid transport profiles would enable estimates of drainage rates, duration of events, and in conjunction with a ponding model (e.g., [Flocco et al., 2010; Eicken et al., 2004]) provide

insight into albedo changes. The resulting input of fresh water into the upper ocean is also an important process which may be tracked through in-ice sensors.

In the Antarctic, snow-ice formation is a significant component of sea ice production. Knowledge of the time evolution of the conductivity–permeability profile in Antarctic sea ice can help delineate regions and time periods conducive to snow-ice formation, e.g., to estimate snow-ice production during storm-driven snowfall events. Like melt ponds in the Arctic, incorporating snow-ice formation into Antarctic sea ice and climate models is critical to improving projections.

Laboratory and field work [Zhou *et al.*, 2013; Loose *et al.*, 2011] have demonstrated the importance of permeability changes in spring in driving a key seasonal transition associated with disproportionate increases in gas transfer, nutrient exchange and biological activity in sea ice. Zhou *et al.* [2013] demonstrated how this important transition enhances primary production within the ice and under the ice through seeding of under-ice waters. Since there is no clear surface expression of these processes, in situ measurement of electrical conductivity (e.g., through arrays sampling large volumes [Jones *et al.*, 2010]) may serve as an important proxy and help track changes in the timing and magnitude of seasonal increases in gas, nutrient and biomass transfer.

6. Conclusions

It has been demonstrated in field experiments conducted in both the Arctic and Antarctic that sea ice exhibits critical behavior in its electrical transport properties at a percolation threshold. Such behavior provides the electrical signature of a key transition in fluid transport properties, known as the *rule of fives*, which determines whether or not

fluid can flow through sea ice. This transition constrains a broad range of processes which are important in the geophysics and biology of the polar regions. The phenomenon is explained theoretically using percolation theory, which provides a universal power law describing the data from both poles, as well as a rigorous link between the fluid and electrical transport properties of sea ice. Our findings open the door to a new generation of techniques for *in situ* analysis and remote monitoring of transport processes, which can improve projections of the fate of Earth's ice packs and the response of polar ecosystems.

Acknowledgments. We are grateful for the support provided by the Division of Mathematical Sciences and the Division of Polar Programs at the US National Science Foundation (NSF) through grants DMS-0537015, DMS-0940249, ARC-0934721, DMS-0940249, DMS-1009704, and DMS-1413454. Joyce Lin was supported by an NSF Postdoctoral Fellowship through a VIGRE grant (DMS-0602219) to the Department of Mathematics at the University of Utah. Adam Gully and Christian Sampson were partially supported by the NSF Research Experiences for Undergraduates (REU) Program through the VIGRE grant. We would like to thank the NSF Math Climate Research Network for their support of this work. We are also thankful for support from the Arctic and Global Prediction Program at the Office of Naval Research through grant N00014-13-10291. This work was also supported in part by the Australian Government through the Antarctic Climate and Ecosystems Cooperative Research Centre. Finally, we thank the crew of the *Aurora Australis* for their help and support during the SIPEX Antarctic expedition. The data used in this paper is freely available by contacting the authors.

References

- Addison, J. (1969), Electrical properties of saline ice, *J. Appl. Phys.*, *40*, 3105–3114.
- Berkowitz, B., and I. Balberg (1992), Percolation approach to the problem of hydraulic conductivity in porous media, *Transport in Porous Media*, *9*, 275–286.
- Buckley, R. G., M. P. Staines, and W. H. Robinson (1986), In situ measurements of the resistivity of Antarctic sea ice, *Cold Reg. Sci. Technol.*, *12*(3), 285–290.
- Druckenmiller, M. L., H. Eicken, M. A. Johnson, D. J. Pringle, and C. C. Williams (2009), Towards an integrated coastal sea-ice observatory: System components and a case study at Barrow, Alaska, *Cold Reg. Sci. Technol.*, *56*, 61–72.
- Eicken, H., T. C. Grenfell, D. K. Perovich, J. A. Richter-Menge, and K. Frey (2004), Hydraulic controls of summer Arctic pack ice albedo, *J. Geophys. Res. (Oceans)*, *109*(C18), C08,007.1–C08,007.12, doi:10.1029/2003JC001989.
- Flocco, D., D. L. Feltham, and A. K. Turner (2010), Incorporation of a physically based melt pond scheme into the sea ice component of a climate model, *J. Geophys. Res.*, *115*, C08,012 (14 pp.), doi:10.1029/2009JC005,568.
- Freitag, J., and H. Eicken (2003), Meltwater circulation and permeability of Arctic summer sea ice derived from hydrological field experiments, *J. Glaciol.*, *49*, 349–358.
- Friedman, A. P., and N. A. Seaton (1998), Critical path analysis of the relationship between permeability and electrical conductivity of three-dimensional pore networks, *Water Resources Res.*, *34*(7), 1703–1710.
- Fritsen, C. H., V. I. Lytle, S. F. Ackley, and C. W. Sullivan (1994), Autumn bloom of Antarctic pack-ice algae, *Science*, *266*, 782–784.

- Fujino, K., and Y. Suzuki (1963), An attempt to estimate the thickness of sea ice by electrical resistivity method ii, *Low Temp. Sci.*, *A21*, 151–157.
- Golden, K. (1990), Convexity and exponent inequalities for conduction near percolation, *Phys. Rev. Lett.*, *65*(24), 2923–2926.
- Golden, K. M., S. F. Ackley, and V. I. Lytle (1998), The percolation phase transition in sea ice, *Science*, *282*, 2238–2241.
- Golden, K. M., H. Eicken, A. L. Heaton, J. Miner, D. Pringle, and J. Zhu (2007), Thermal evolution of permeability and microstructure in sea ice, *Geophys. Res. Lett.*, *34*, L16,501 (6 pages and issue cover), doi:10.1029/2007GL030,447.
- Haas, C. (2004), Late-summer sea ice thickness variability in the Arctic Transpolar Drift 1991-2001 derived from ground-based electromagnetic sounding, *Geophys. Res. Lett.*, *31*, L09,402, doi:10.1029/2007GL030,447.
- Halperin, B. I., S. Feng, and P. N. Sen (1985), Differences between lattice and continuum percolation transport exponents, *Phys. Rev. Lett.*, *54*(22), 2391–2394.
- Ingham, M., D. J. Pringle, and H. Eicken (2008), Cross-borehole resistivity tomography of sea ice, *Cold Reg. Sci. Technol.*, *52*, 263–277, 10.1016/j.coldregions.2007.05.002.
- Jones, K. A., M. Ingham, D. J. Pringle, and H. Eicken (2010), Temporal variations in sea ice resistivity: resolving anisotropic microstructure through cross-borehole dc resistivity tomography, *J. Geophys. Res.*, *115*, C11,023, doi:10.1029/2009JC006,049.
- Loose, B., L. A. Miller, S. Elliott, and T. Papakyriakou (2011), Sea ice biogeochemistry and material transport across the frozen interface, *Oceanography*, *24*(3), 202–218, <http://dx.doi.org/10.5670/oceanog.2011.72>.

Lytle, V. I., and S. F. Ackley (1996), Heat flux through sea ice in the Western Weddell Sea:

Convective and conductive transfer processes, *J. Geophys. Res.*, *101*(C4), 8853–8868.

Maksym, T., and T. Markus (2008), Antarctic sea ice thickness and snow-to-ice conversion

from atmospheric reanalysis and passive microwave snow depth, *J. Geophys. Res.*, *113*,

C02S12, doi:10.1029/2006JC004,085.

Meier, W. N., G. K. Hovelsrud, B. E. H. van Oort, J. R. K. M. Kovacs, C. Michel, C. Haas,

M. A. Granskog, S. Gerland, D. K. Perovich, A. Makshtas, and J. D. Reis (2014), Arctic

sea ice in transformation: A review of recent observed changes and impacts on biology

and human activity, *Rev. Geophys.*, *51*, 185–217, doi:10.1002/2013RG000,431.

Perovich, D. K., T. C. Grenfell, B. Light, and P. V. Hobbs (2002), Seasonal evolution

of the albedo of multiyear Arctic sea ice, *J. Geophys. Res. (Oceans)*, *107*(C10), 8044,

doi:10.1029/2000JC000,438.

Perovich, D. K., B. Light, H. Eicken, K. F. Jones, K. Runciman, and S. V. Nghiem

(2007), Increasing solar heating of the Arctic Ocean and adjacent seas, 1979-2005:

Attribution and role in the ice-albedo feedback, *Geophys. Res. Lett.*, *34*, L19,505,

doi:10.1029/2007GL031,480.

Petrich, C., and H. Eicken (2009), Growth, structure and properties of sea ice, in *Sea Ice*,

edited by D. N. Thomas and G. S. Dieckmann, pp. 23–77, Wiley-Blackwell.

Pistone, K., I. Eisenman, and V. Ramanathan (2014), Observational determination of

albedo decrease caused by vanishing arctic sea ice, *Proc. Natl. Acad. Sci.*, *111*(9), 3322–

3326.

- Polashenski, C., D. Perovich, and Z. Courville (2012), The mechanisms of sea ice melt pond formation and evolution, *J. Geophys. Res. C (Oceans)*, *117*, C01,001 (23 pp.), doi:10.1029/2011JC007,231.
- Pringle, D. J., J. E. Miner, H. Eicken, and K. M. Golden (2009), Pore-space percolation in sea ice single crystals, *J. Geophys. Res. (Oceans)*, *114*, C12,017, 12 pp., doi:10.1029/2008JC005,145.
- Reid, J. E., A. Pfaffling, A. P. Worby, and J. R. Bishop (2006), In situ measurements of the direct-current conductivity of Antarctic sea ice: Implications for airborne electromagnetic sounding of sea-ice thickness, *Ann. Glaciol.*, *44*, 217–223.
- Rysgaard, S., R. N. Glud, M. K. Sej, J. Bendtsen, and P. B. Christensen (2007), Inorganic carbon transport during sea ice growth and decay: A carbon pump in polar seas, *J. Geophys. Res.*, *112*, C03,016, doi:10.1029/ 2006JC003,572.
- Sampson, C., K. M. Golden, A. Gully, and A. P. Worby (2011), Surface impedance tomography for Antarctic sea ice, *Deep Sea Res. II*, *58*, 1149–1157.
- Serreze, M. C., M. M. Holland, and J. Stroeve (2007), Perspectives on the Arctic’s shrinking sea-ice cover, *Science*, *315*, 1533–1536.
- Stauffer, D., and A. Aharony (1992), *Introduction to Percolation Theory, Second Edition*, Taylor and Francis Ltd., London.
- Stogryn, A., and G. J. Desargant (1985), The dielectric properties of brine in sea ice at microwave frequencies, *IEEE Trans. Antennas Propagat.*, *AP-33*(5), 523–532.
- Thomas, D. N., and G. S. Dieckmann (Eds.) (2009), *Sea Ice, 2nd Edition*, Wiley-Blackwell, Oxford.

- 323 Thyssen, F., H. Kohnen, M. V. Cowan, and G. W. Timco (1974), DC resistivity measure-
324 ments on the sea ice near pond inlet, *Polarforschung*, 44, 117–126.
- 325 Wong, P. (1988), The statistical physics of sedimentary rocks, *Physics Today*, 41(12),
326 24–32.
- 327 Zhou, J., B. Delille, H. Eicken, M. Vancoppenolle, F. Brabant, G. Carnat, N.-X. Geilfus,
328 T. Papakyriakou, B. Heinesch, and J.-L. Tison (2013), Physical and biogeochemical
329 properties in landfast sea ice (Barrow, Alaska): Insights on brine and gas dynamics
330 across seasons, *J. Geophys. Res. Oceans*, 118, 3172–3189, doi:10.1002/jgrc.20,232.

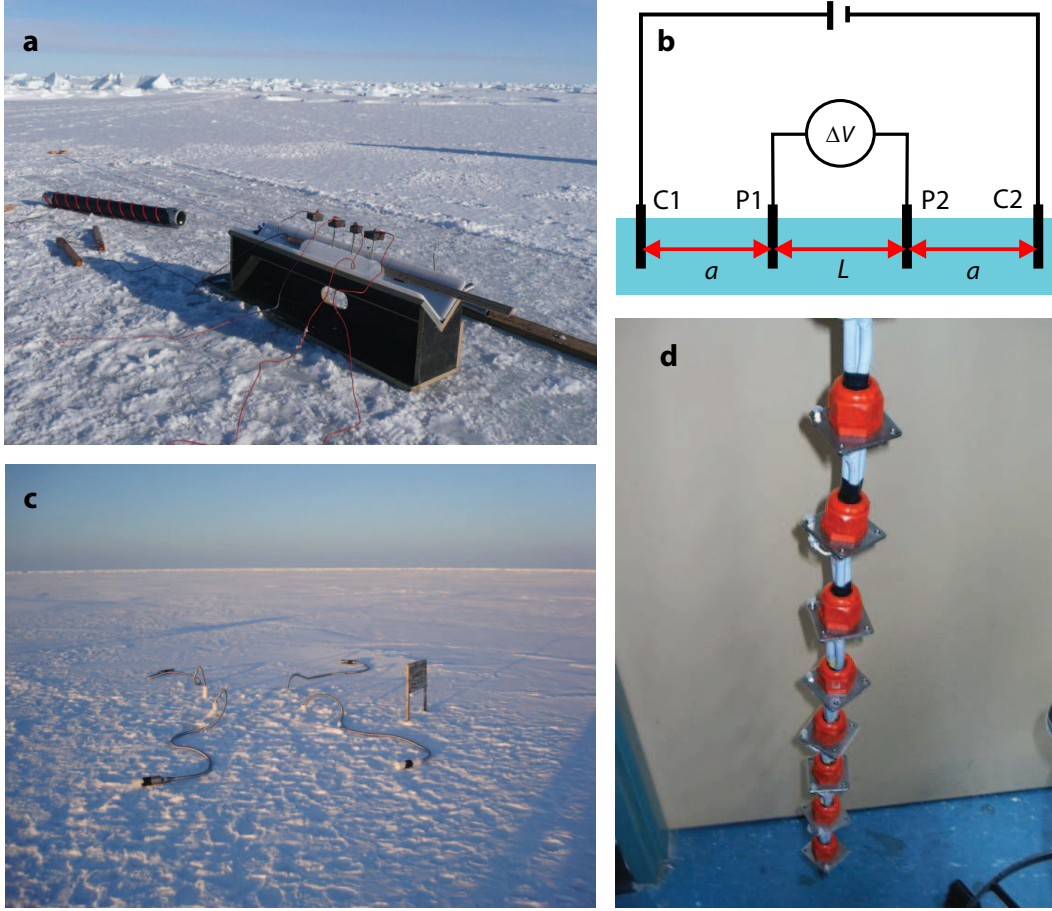


Figure 1. (a) A Wenner electrode array is configured to measure the vertical conductivity of Antarctic sea ice, by inserting the four probes into an extracted ice core. (b) A current I is injected into the core through the outer electrodes C1 and C2. The potential difference ΔV resulting from the current flow is measured by the inner electrodes P1 and P2. The ratio $\Delta V/I$ is the resistance R in ohms. Here the electrode spacing is $L = 10$ cm and $a = 10$ cm. (c) A cross-borehole array is frozen into Arctic sea ice. The DC resistivity profile was tomographically reconstructed in the volume enclosed by the electrode strings. One of the strings, with 10 cm separation of the plates, is shown in (d).

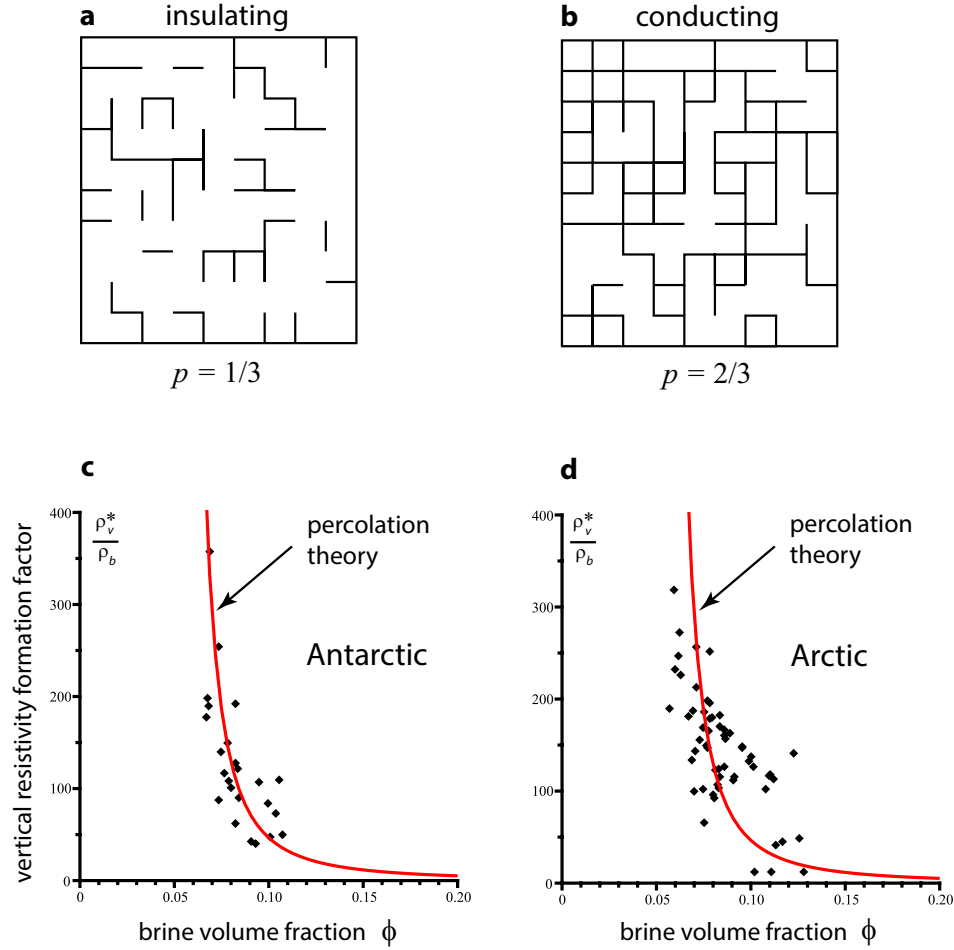


Figure 2. The two dimensional square lattice below its percolation or connectivity threshold $p_c = 1/2$ in (a), and above in (b). We display the vertical resistivity formation factor data from the Antarctic in (c) and the Arctic in (d), along with the same prediction from percolation theory in each. Both data and theory exhibit divergent behavior as ϕ approaches $\phi_c \approx 0.05$ from the right, with a vertical asymptote at $\phi = \phi_c$, electrically signaling the transition to relatively impermeable ice.

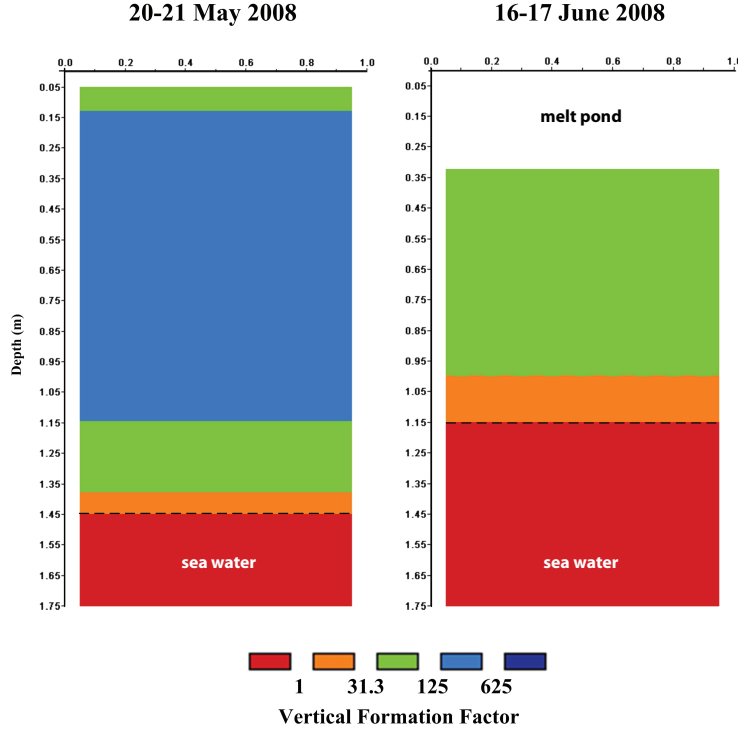


Figure 3. Cross-borehole tomographic reconstructions of the vertical resistivity formation factor for Arctic sea ice before (a) and after (b) melt pond formation. The evolution of resistivity structure is consistent with warming of the ice, thus increasing the fluid permeability and facilitating the infiltration of meltwater into the upper layer of sea ice from the surface. To connect the electrical properties of sea ice to its important processes, the range of the resistivity formation factor G is divided into five regimes: $G > 625$ (ice impermeable enough to allow ponds to grow for surface ablation rates of 10 cm/d or larger for a critical pore radius of 0.1 mm); $125 < G \leq 625$, blue (ice impermeable enough to allow ponds to grow for surface ablation rates between 10 and 50 cm/d for a critical pore radius of 0.1 mm); $31.3 < G \leq 125$, green (at formation factors of 31.3 or larger ice is impermeable from the perspective of CO_2 exchange and build-up of nutrients and biomass in the ice [Rysgaard *et al.*, 2007], and sufficiently impermeable to drainage to support surface ponding); $1 < G \leq 31.3$, orange (highly permeable ice that allows for CO_2 pumping and build-up of nutrients and biomass); $G \leq 1$, red (assumed to be free water column). Only the most resistive ice $G > 625$ is not shown.